

## Supporting Information

### **Photoelectrochemical two-dimensional electronic spectroscopy (PEC2DES) of photosystem I to study charge separation dynamics in photosynthesis**

Manuel López-Ortiz<sup>1,#</sup>, Luca Bolzonello<sup>2,#</sup>, Matteo Bruschi<sup>3</sup>, Elisa Fresch<sup>3</sup>, Elisabetta Collini<sup>3</sup>, Chen Hu<sup>4</sup>, Roberta Croce<sup>4</sup>, Niek F. van Hulst<sup>2,5,\*</sup>, Pau Gorostiza<sup>1,5,6,\*</sup>

<sup>1</sup> *Institute for Bioengineering of Catalonia (IBEC), The Barcelona Institute of Science and Technology, Barcelona, 08028 Spain.*

<sup>2</sup> *ICFO - Institut de Ciències Fotòniques, The Barcelona Institute of Science and Technology, Castelldefels, Barcelona, 08860 Spain.*

<sup>3</sup> *Dipartimento di Scienze Chimiche, Università degli Studi di Padova, Padova, 35131 Italy.*

<sup>4</sup> *Biophysics of Photosynthesis, Department of Physics and Astronomy, Faculty of Sciences, Vrije Universiteit Amsterdam, De Boelelaan 1081, Amsterdam 1081 HV, The Netherlands.*

<sup>5</sup> *ICREA - Institució Catalana de Recerca i Estudis Avançats, Barcelona, 08010 Spain.*

<sup>6</sup> *CIBER-BBN, Barcelona 08028, Spain.*

*# These authors contributed equally.*

*\* Corresponding authors. E-mail: [niek.vanhulst@icfo.eu](mailto:niek.vanhulst@icfo.eu) (N. F. van H.), [pau@icrea.cat](mailto:pau@icrea.cat) (P. G.)*

#### CONTENTS:

SI1. PSI-LHCI complexes purification

SI2. Au-pIQA-cys-PSI-LHCI electrode preparation

SI3. AFM characterization Au-pIQA-cys-PSI-LHCI biohybrid electrode

SI4. Acquisition and setup details

SI5. Phase modulation

SI6. Dazzler intensity artifact

SI7. Incoherent mixing, linear reconstruction

SI8. Incoherent mixing, evolution along  $t_2$

SI9: Custom electrochemical cell design

SI10: Pulse compression

## **SI1. PSI-LHCI complexes purification:**

Arabidopsis thaliana plants (Arabidopsis Col-0) were grown under white light at  $120 \mu\text{mol photons}\cdot\text{m}^{-2}\cdot\text{s}^{-1}$ , 12 hr/12hr day/night cycle at  $23 \text{ }^\circ\text{C}$ , for 5 weeks. Thylakoid membranes were isolated from Arabidopsis leaves according to s PSI-LHCI complexes were purified from thylakoid membranes with sucrose density gradients as previously described<sup>4</sup>. Chlorophyll concentration was adjusted to  $0.5 \text{ mg Chl}\cdot\text{ml}^{-1}$  in  $5 \text{ mM EDTA}$ ,  $10 \text{ mM Hepes pH } 7.5$  and solubilized with an equal amount of detergent solution ( $1\% \alpha$ -decylmaltoside (DM) in  $10 \text{ mM Hepes } 7.5$ ) for 10 min. After solubilization, the sample was centrifuged at  $12,000 \times g$ , for 10 min to eliminate the insolubilized material. The supernatant was loaded onto the sucrose gradients prepared by freezing and thawing a sucrose solution ( $500\text{mM}$  sucrose,  $20 \text{ mM Hepes pH } 7.5$ ,  $0.06\% \alpha$ -DM). The gradients were centrifuged for 16 h at  $4 \text{ }^\circ\text{C}$  at  $160,000 \times g$ . PSI-LHCI complexes were collected with a syringe. PSI-LHCI samples chlorophyll concentration is  $0.28 \mu\text{g}\cdot\mu\text{l}^{-1}$ .

## **SI2. Au-pIQA-cys-PSI-LHCI electrode preparation**

Transparent gold electrodes AuTr10 (Dropsens-Metrohm, Spain) were sonicated in ethanol before use. Electrodes were dried in nitrogen stream prior to incubation of linker peptide pIQA-cys  $0.1 \text{ mM}$ , in sodium acetate buffer  $50 \text{ mM}$ ,  $\text{pH } 4.5$ , for 30 min at room temperature. After peptide incubation, electrodes were gently rinsed with Phosphate Buffer Saline (PBS)  $50 \text{ mM}$ ,  $\text{pH } 7.4$ . Droplets of  $5 \mu\text{l}$  of PSI-LHCI sample ( $1.4 \mu\text{g}$  chlorophyll) were incubated in the electrode surface in the dark at  $4^\circ\text{C}$  for 1h.

## **SI3. AFM characterization Au-pIQA-cys-PSI-LHCI biohybrid electrode**

Atomic force microscopy (AFM) imaging. AFM scans were performed using an MFP-3D atomic force microscope (Asylum Research, Santa Barbara, CA) using V-shaped  $\text{Si}_3\text{N}_4$  cantilevers with sharp silicon tips and having a nominal spring constant of  $0.12 \text{ N}\cdot\text{m}^{-1}$  (SNL, Bruker AFM Probes, Camarillo, CA). The AFM was operated in tapping mode in liquid, covering the sample with PBS  $50 \text{ mM}$ ,  $\text{pH } 7.4$ .

## **SI4. Acquisition and setup details**

Along  $t_1$  and  $t_3$ , they are collected from 0 to 48 fs every 4 fs, while along  $t_2$  from 0 to 450fs every 15 fs, generating 3d matrices of  $13 \times 13 \times 31$  points. We select a rotating frame at  $t_2=60\text{fs}$  are shown, the signal is completely decayed within 48 fs along  $t_1$  and  $t_3$ , justifying our choice of stop at 48 the acquisition. The step of 4 fs along coherence time is suitable for a bandwidth of  $4000 \text{ cm}^{-1}$  respecting Nyquist limit. Therefore, using appropriate rotating frame ( $13342 \text{ cm}^{-1}/0.4 \text{ fs}^{-1}$ ), it is possible to get all the responses within our laser spectrum (ranging from  $\sim 14000$  to  $\sim 17000 \text{ cm}^{-1}$ ).

The tuning of the laser fluence in the experiment was determined by several factors: the number of excitations per PSI-LHCI, the minimization of the Dazzler artifact, sample degradation, and the signal-to-noise ratio of the non-linear signal. The first three factors impose limitations that we could not exceed to ensure the validity of the experiment. Additionally, the energy per pulse had to be maintained above a certain threshold to prevent the generated current from falling below the noise level.

To cope with these constraints, we opted for a large beam ( $\sim 2.5 \text{ mm}$  in diameter), which allowed us to uniformly excite the PSI-LHCI sample across the electrode and maximize the current, while avoiding the pure linear regime. Through this careful optimization, we arrived at an energy of approximately  $50 \text{ nJ}$  per pulse.

### SI5. Phase modulation

The phase modulation using Dazzler has already been described in previous work<sup>1</sup>.

The modulation is based on evolving individual phases of the 4 pulses at every laser repetition with a different step. Different combinations of modulation frequencies ( $f_n$ ) are linked to different combination of phases of the response of the system, that in turn is connected to the response frequencies combinations :  $\pm f_1 \pm f_2 \pm f_3 \pm f_4 \rightarrow \pm \varphi_1 \pm \varphi_2 \pm \varphi_3 \pm \varphi_4 \rightarrow \pm \omega_1 \pm \omega_2 \pm \omega_3 \pm \omega_4$ .

The table below summarize the different combination and frequencies.

component	divisors	Frequency (Hz)
<i>linear</i>		
$f_{21}$	6-0	250
$f_{31}$	8-0	333.33
$f_{41}$	9-0	375
$f_{32}$	8-6	83.33
$f_{42}$	9-6	125
$f_{43}$	9-8	41.66
<i>4<sup>th</sup> order</i>		
$f_{\text{reph}}$	-0+6+8-9	208.33
$f_{\text{non-reph}}$	-0+6-8+9	291.66
$f_{2Q}$	-0-6+8+9	458.33

Table SI-1

SO, rephasing and non rephasing signals are extracted at 208.33 and 291.66 Hz respectively and the linear signal shown in the main text at 250 Hz.

### SI6. Dazzler intensity artifact

It has been reported that Dazzler generates artifacts in population detected 2DES especially in the rephasing signal<sup>2</sup>. This artifact affects the shape of the rephasing spectrum maps in time domain displaying a constant signal on the diagonal ( $t_1=t_3$ ) and has shown to be constant also along the delay time  $t_2$ . Potential artifacts have been limited comparing PEC2DES with a control signal measuring excitation intensity simultaneously acquired with a linear detector (see below). Uneven excitation is not responsible for the overall PEC2DES signal as photo-diode signal has a different shape with respect to photo-current response.

The Dazzler has limited capabilities in keeping constant intensity while changing phases of a quartet of pulse. This give rise to nonlinearities that are not dependent on the response of the sample but on the fluctuant intensity of excitation. This effect, mainly present in the rephasing signal, has already been reported in the PhD thesis of Roeding S. from the group of Brixner<sup>2</sup>. They correct this effect by iteratively searching for intensity correction factor at any collection point, until a linear response sample gives no non-linear effect.

We adopted instead a a posteriori approach where we detect the linear response of a photodiode simultaneously with the experiment and making a properly normalized subtraction of the photodiode generated feature.

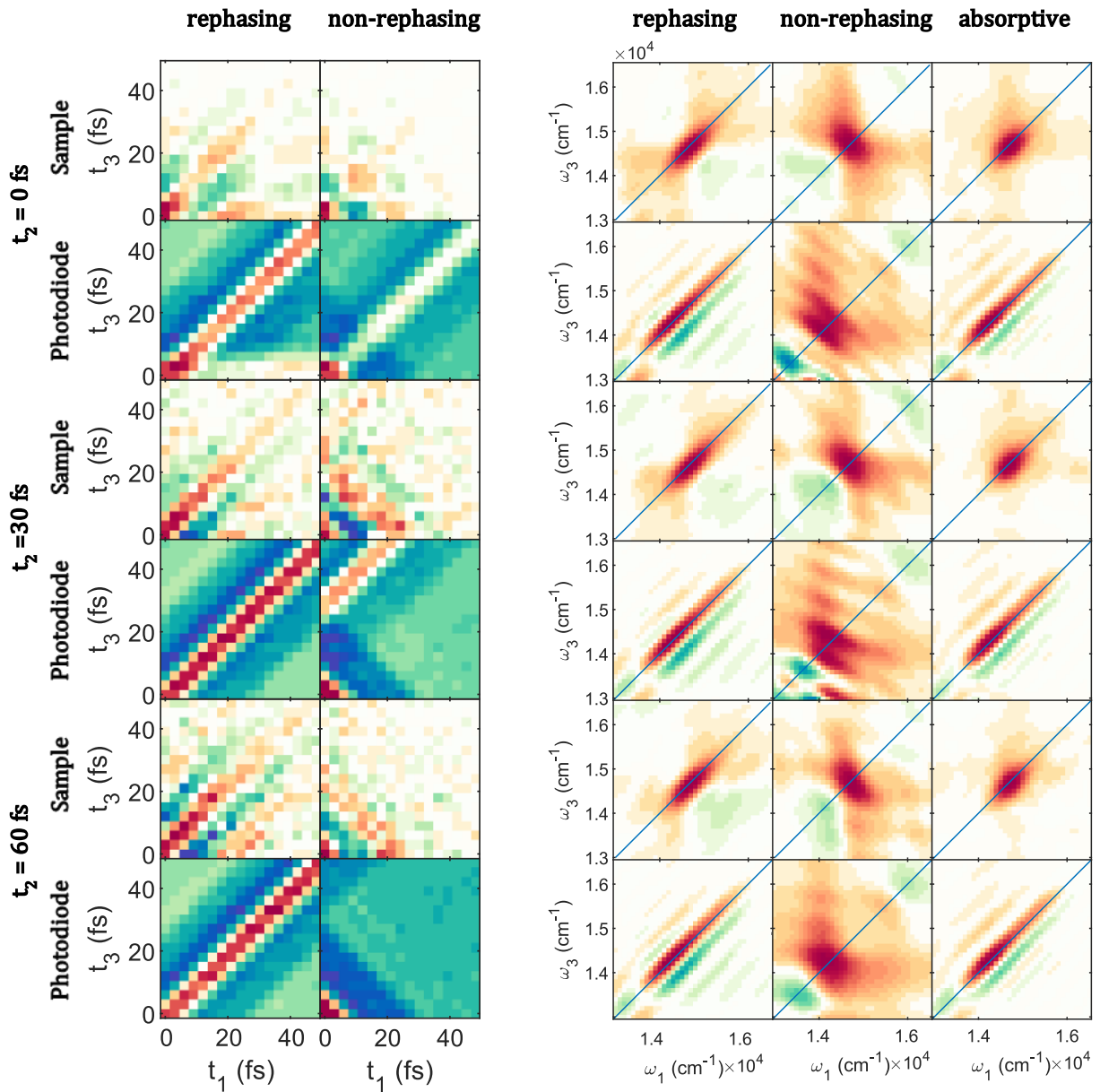


Figure SI-F1 Signal coming from sample and photodiode at different  $t_2$ . The time-dependent photodiode rephasing signal shows a constant feature along the diagonal that does not decrease increasing coherence times. This leads to a frequency dependent signal distributed along the diagonal that will depend on the coherence time range used. In the sample signal the photodiode collected artifact is removed, and the remaining signal decays showing the typical shape in the frequency domain. Moreover, note that in the time dependent non-rephasing the artifact disappears when  $t_2$  is larger than coherence time range. In the frequency dependent non-rephasing the peak is shifted with respect to the sample confirming that the signal from the sample is not due to dazzler artifact.

## SI7. Incoherent mixing, linear reconstruction

Incoherent mixing is an effect that takes place when the detected signal is not proportional to the population generated by the quartet of pulses which is the first principle of population detected 2DES. This proportionality will not hold if excitons, or eventually charges, interact and annihilate between each other before being detected. In the latter case, part of the linear signal falls into the modulated detection frequencies of rephasing and non-rephasing signals. This contribution is constant along  $t_2$  and thus would fit well our situation. The reconstructed linear signal into the 2D maps (see Supplementary below) has similar shape to rephasing and non-rephasing maps but is expected to have opposite sign. Moreover, the presence of the vibrational coherence and the different intensity of rephasing and non-rephasing signals suggest that, at least in part, non-linear signal is present in the detected frequencies. A way to evaluate the amount of coherent mixing is to compare the non-linear spectrum with the reconstructed linear on the  $t_1$ - $t_3$  map using equations 28 and 29 found in Gregoire et al. paper<sup>3</sup>

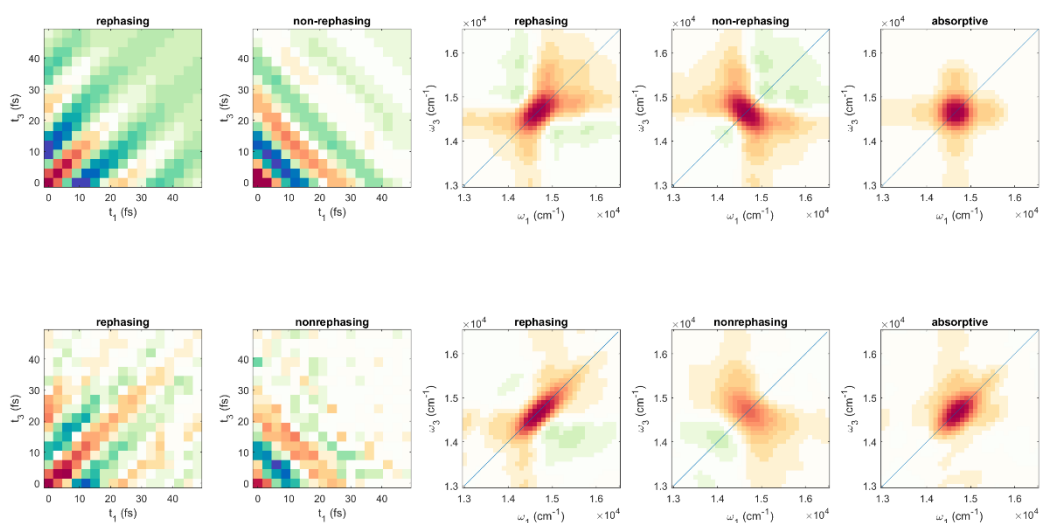


Figure SI-F2 Linear signal reconstruction (top row) and actual acquired signal at  $t_2 = 60$  fs (bottom row).

The comparison between the reconstructed linear signal and the acquired ones. The shapes of rephasing and non-rephasing are very similar in between each other. However, the intensity ratio between rephasing and non-rephasing is different (as expected for a non-linear response, because of the slower decay along coherence time of the rephasing signal) giving rise to different absorptive maps. The non-linear is indeed elongated along the diagonal.

## SI8. Incoherent mixing, evolution along $t_2$ .

As seen in figure 3 in the main document, the dynamics along the population time are almost flat. We performed anyway the global fit using an oscillation component that outputs the CAS at  $750 \text{ cm}^{-1}$ . That's the only CAS obtainable from the fitting that has a distribution of amplitudes (shape) that resemble the 2d signal. We show in figure SI-F3 that the Fourier analysis performed on the residuals of a global exponential fitting (only real) in different positions are very noisy, but all of them contain the  $750 \text{ cm}^{-1}$  component.

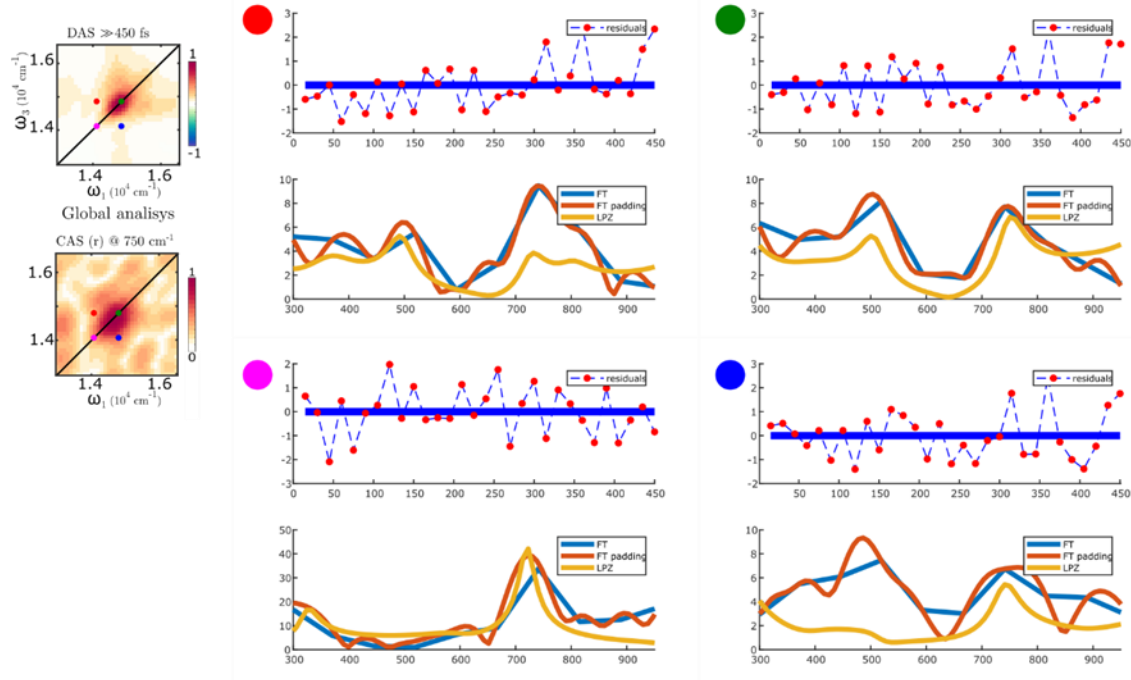


Figure SI-F3 Fourier analysis of the residuals of an only real exponential global fitting. The 750 component is present with every technique in all the positions.

### SI9. Custom electrochemical cell design

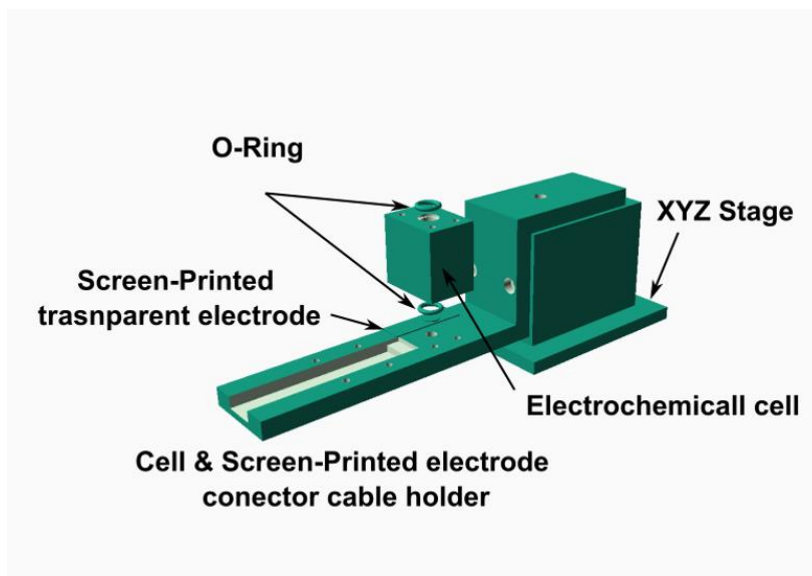


Figure SI-F3 Blueprint of electrochemical cell and screen-printed electrode holder adapted to spectro-electrochemical set-up.

## SI10. Pulse compression

Pulse duration ( $\sim 10$  fs) was measured by exploiting standard sum frequency signal (FROG) generated on a  $10\ \mu\text{m}$  BBO crystal.

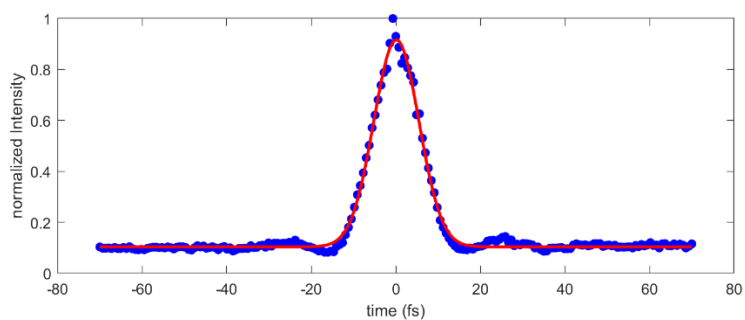


Figure SI-F4 Frog trace from -70 to +70 fs.

1. Bolzonello, L. *et al.* Photocurrent-Detected 2D Electronic Spectroscopy Reveals Ultrafast Hole Transfer in Operating PM6/Y6 Organic Solar Cells. *J. Phys. Chem. Lett.* **12**, 3983–3988 (2021).
2. Röding, S. Coherent multidimensional spectroscopy in molecular beams and liquids using incoherent observables. *PhD Thesis* (2017).
3. Grégoire, P. *et al.* Incoherent population mixing contributions to phase-modulation two-dimensional coherent excitation spectra. *J. Chem. Phys.* **147**, (2017).
4. Caffarri, S., Kouřil, R., Kereiče, S., Boekema, E. J. & Croce, R. Functional architecture of higher plant photosystem II supercomplexes. *EMBO J.* **28**, 3052–3063 (2009).